TNCF MODEL EXPLANATION OF COLD FUSION PHENOMENON IN SURFACE LAYERS OF CATHODES IN ELECTROLYTIC EXPERIMENTS

H. Kozima[1]*, J. Warner[1], C. Salas Cano[1] and J. Dash[1]

ABSTRACT

Changed isotope concentrations and distorted surface topographies were observed by J. Dash et al. over the last ten years in the surface layers of cathodes after electrolytic experiments. These results can now be understood in terms of the "trapped neutron" catalyzed fusion (TNCF) model, which invokes no more than standard nuclear physics and the natural capability of background neutrons in the laboratory to initiate spontaneous nuclear transmutations by thermal neutron absorption. The cathodes exhibited intricate microscopic features in the areas where the altered isotope concentrations had been detected. We postulate that these features were caused by nuclear transmutation (NT). In the experiments where new elements were found or where the concentrations of the host cathodes isotope ratios were scrambled excess treat was generally given off as well, in amounts that were, very tiny but statistically significant and certainly incommensurate with any enthalpies that could be attributed to ordinary chemical processes. The products of nuclear transmutation are explained either by decay of the cathode element nuclei with one higher mass number than original (nuclear transmutation by decay, or NTD) or by fissions of these nuclei with several more mass numbers (nuclear transmutation by fission, or NTF). The model analysed two cases of quantitative changes of isotope ratios in Ti and Pd cathodes. The result shows that explanation of the experimental data sets as a whole is possible with reasonable values of the adjustable parameter in the model;

$$n_n = 1.25 \times 10^{13}\ \mathrm{cm}^{-3}, \quad \text{(Ti)},$$
$$n_n = 4 \times 10^{12}\ \mathrm{cm}^{-3}. \quad \text{(Pd)},$$

For the characteristic surface topography with craters of diameters 1 μm, a possible semi-quantitative explanation is given in terms of explosions of tiny spheres (droplets) locally heated by nuclear reactions in the droplet with the parameter given above.

1. INTRODUCTION

J. Dash et al. at Portland State University have performed many cold fusion (CF) experiments with electrolytic systems containing cathodes of Pd, Ti, and Ni and electrolytes containing H_2SO_4 dissolved in both heavy (D_2O) and light (H_2O) water. [1–11] They have measured exiguous but appreciable amounts of excess heat and found new elements, generally localized at pits or craters

[1] Physics Department and Low Energy Nuclear Laboratory, Portland State Univ., Portland, OR 97207-0751, USA
E-mail address cf-lab.kozima@pdx.edu
* On leave from Cold Fusion Research Laboratory, Yatsu 597-16, Shizuoka, Shizuoka 421-1202, Japan.
E-mail: cf-lab.Kozima@nifty.ne.jp

in the surface layer of cathodes, and present up to a depth of about 1 μm. These elements are explainable by the beta decay of unstable, short-lived nuclei that are formed when cathode elements absorb a trapped neutron. This process, which is one of the many examples of reactions explainable by the TNCF model, can be called nuclear transmutation by decay. [12–14]

The number of events (reactions) N_x between the "trapped neutrons" and the lattice nuclei ${}^{A}_{Z}X$ during a time τ in a volume V of a reaction region is given by the equation (Eq. (11.20) in the paper [12] or Eq.(3) in the paper [13]):

$$N_X = 0.35\, n_n v_n n_x V \sigma_{nX}\, \tau\, \xi, \tag{1}$$

where n_n and n_x are the densities of the "trapped neutrons" and the X nuclei, respectively, v_n is the thermal velocity of the trapped neutron, σ_{nX} is the cross section of the reaction defined in free space by standard nuclear physics, and ξ is the instability parameter specifying the feasibility of the reaction in a lattice. It is taken as 1 (ξ= 1) if the reaction occurs with the same probability as in free space, and zero if the reaction does not occur at all in the lattice.

Nuclear reactions between lattice nuclei ${}^{A}_{Z}X$ and trapped neutrons which are relevant to the experimental systems treated in the above experiments [1–11] are listed as follows with data of the reaction in parentheses next to the reaction formula (natural abundance of initial nuclide ${}^{A}_{Z}X$ in %, σ_{nX} in barns (1 b = 10^{-24} cm^2), and the decay constant τ_d of β decay or electron capture [15] if the resulting nucleus ${}^{A+1}_{Z}X^*$ is unstable; s = second, m = minute, h = hour, d = day and y = year):

$$n + {}^{26}_{12}\mathrm{Mg} = {}^{27}_{12}\mathrm{Mg}^* = {}^{27}_{13}\mathrm{Al} + e^- + \underline{\nu}_e, \ (11.17\%,\ 0.038\ \mathrm{b},\ 9.5\ \mathrm{m}) \tag{2}$$

$$n + {}^{34}_{16}\mathrm{S} = {}^{35}_{16}\mathrm{S}^* = {}^{35}_{17}\mathrm{Cl} + e^- + \underline{\nu}_e, \ (4.22\%,\ 0.225\ \mathrm{b},\ 87.51\ \mathrm{d}) \tag{3}$$

$$n + {}^{44}_{20}\mathrm{Ca} = {}^{45}_{20}\mathrm{Ca}^* = {}^{45}_{21}\mathrm{Sc} + e^- + \underline{\nu}_e, \ (2.06\%,\ 0.884\ \mathrm{b},\ 163.8\ \mathrm{d}) \tag{4}$$

$$n + {}^{45}_{21}\mathrm{Sc} = {}^{46}_{21}\mathrm{Sc}^* = {}^{46}_{22}\mathrm{Ti} + e^- + \underline{\nu}_e, \ (100\%,\ 27.14\ \mathrm{b},\ 83.79\ \mathrm{d}) \tag{5}$$

$$n + {}^{50}_{22}\mathrm{Ti} = {}^{51}_{22}\mathrm{Ti}^* = {}^{51}_{23}\mathrm{V} + e^- + \underline{\nu}_e, \ (5.34\%,\ 0.179\ \mathrm{b},\ 5.76\ \mathrm{m}) \tag{6}$$

$$n + {}^{51}_{23}\mathrm{V} = {}^{52}_{23}\mathrm{V}^* = {}^{52}_{24}\mathrm{Cr} + e^- + \underline{\nu}_e, \ (99.76\%,\ 4.9\ \mathrm{b},\ 3.75\ \mathrm{m}) \tag{7}$$

$$n + {}^{58}_{28}\mathrm{Ni} = {}^{59}_{28}\mathrm{Ni}^* = {}^{58}_{29}\mathrm{Co} + e^- + \underline{\nu}_e, \ (67.88\%,\ 4.503\ \mathrm{b},\ 7.8 \times 10^4\ \mathrm{y}) \tag{8}$$

$$n + {}^{62}_{28}\mathrm{Ni} = {}^{63}_{28}\mathrm{Ni}^* = {}^{63}_{29}\mathrm{Cu} + e^- + \underline{\nu}_e, \ (3.66\%,\ 414.20\ \mathrm{b},\ 100.1\ \mathrm{y}) \tag{9}$$

$$n + {}^{63}_{29}\mathrm{Cu} = {}^{64}_{29}\mathrm{Cu}^* = {}^{64}_{30}\mathrm{Zn} + e^- + \underline{\nu}_e, \ (69.09\%,\ 4.51\ \mathrm{b},\ 12.7\ \mathrm{h}) \tag{10}$$

$$n + {}^{64}_{28}\mathrm{Ni} = {}^{65}_{28}\mathrm{Ni}^* = {}^{65}_{29}\mathrm{Cu} + e^- + \underline{\nu}_e, \ (1.08\%,\ 14.80\ \mathrm{b},\ 2.51\ \mathrm{h}) \tag{11}$$

$$n + {}^{65}_{29}\mathrm{Cu} = {}^{66}_{29}\mathrm{Cu}^* = {}^{66}_{30}\mathrm{Zn} + e^- + \underline{\nu}_e, \ (30.91\%,\ 2.168\ \mathrm{b},\ 5.1\ \mathrm{m}) \tag{12}$$

$$n + {}^{106}_{46}\mathrm{Pd} = {}^{107}_{46}\mathrm{Pd}^* = {}^{107}_{47}\mathrm{Ag} + e^- + \underline{\nu}_e, \ (27.33\%,\ 0.303\ \mathrm{b},\ 6.5 \times 10^6\ \mathrm{y}) \tag{13}$$

$$n + {}^{107}_{47}\mathrm{Ag} = {}^{108}_{47}\mathrm{Ag}^* = {}^{108}_{48}\mathrm{Cd} + e^- + \underline{\nu}_e, \ (51.82\%,\ 38.6\ \mathrm{b},\ 2.37\ \mathrm{m}) \tag{14}$$

$$n + {}^{108}_{46}\mathrm{Pd} = {}^{109}_{46}\mathrm{Pd}^* = {}^{109}_{47}\mathrm{Ag} + e^- + \underline{\nu}_e, \ (26.71\%,\ 8.5\ \mathrm{b},\ 4.696\ \mathrm{m}) \tag{15}$$

$$n + {}^{109}_{47}\mathrm{Ag} = {}^{110}_{47}\mathrm{Ag}^* = {}^{110}_{48}\mathrm{Cd} + e^- + \underline{\nu}_e, \ (48.18\%,\ 90.53\ \mathrm{b},\ 24.6\ \mathrm{s}) \tag{16}$$

$$n + {}^{110}_{46}\mathrm{Pd} = {}^{111}_{46}\mathrm{Pd}^* = {}^{111}_{47}\mathrm{Ag}^* + e^- + \underline{\nu}_e, \ (11.81\%,\ 0.227\ \mathrm{b},\ 5.5\ \mathrm{h}) \tag{17}$$

$${}^{111}_{47}\mathrm{Ag}^* = {}^{111}_{48}\mathrm{Cd} + e^- + \underline{\nu}_e, \ (7.45\ \mathrm{d}) \tag{18}$$

$$n + {}^{196}_{78}\mathrm{Pt} = {}^{197}_{78}\mathrm{Pt}^* = {}^{197}_{79}\mathrm{Au} + e^- + \underline{\nu}_e, \ (25.3\%,\ 0.9\ \mathrm{b},\ 95.4\ \mathrm{m}) \tag{19}$$

$$n + {}^{198}_{78}\mathrm{Pt} = {}^{199}_{78}\mathrm{Pt}^* = {}^{199}_{79}\mathrm{Au}^* + e^- + \underline{\nu}_e, \ (7.21\%,\ 4.0\ \mathrm{b},\ 30.8\ \mathrm{m}) \tag{20}$$

$${}^{199}_{79}\mathrm{Au}^* = {}^{199}_{80}\mathrm{Hg} + e^- + \underline{\nu}_e, \ (3.139\ \mathrm{d}) \tag{21}$$

Using these nuclear reactions, we analyze experimental data [l-11] obtained by J. Dash et al. A short paper about this work presented at ICCF9 will be published in the Proceedings of ICCF9. [16]

2. EXPERIMENTAL DATA SETS

J. Dash et al. have worked on electrolytic systems with cathodes of Pd, Ti and Ni and electrolytes of H_2SO_4 dissolved in both D_2O and H_2O. [1-11] We summarize their results with the following short-hand notation:

[Cathode/Solvent(s)/Electrolyte/Anode//Method//Result(s)].[Reference]

2.1 Surface Topography of Cathodes [l-5,7, 9-11]

The surface topography was analyzed before and after the experiments using a scanning electron microscope (SEM) with an attached energy dispersive spectrometer (EDS), an atomic force microscope (AFM), and (at times) a scanning tunneling microscope (STM) as well. In some cases, localized regions in the surface layer of the cathodes of Pd, Ti, and Ni exhibited the topographic characteristics of super-heating:

[Pd/H_2O, D_2O/H_2SO_4/Pt//SEM, STM, AFM//Rimmed craters]. [1]

[Pd/H_2O, D_2O/H_2SO_4/Pt//SEM, STM, AFM//Rimmed craters]. [2]

[Pd/H_2O, D_2O/H_2SO_4/Pt//SEM, EDS//Island structure, localized melting]. [3]

To our knowledge, these experiments constituted the first time that clear and detailed microscopic structures were detected in the near surface region after a cold fusion phenomenon (CFP), something that implies super-heating, and suggests that the nuclear reactions may have actually taken place in the surface layers. A semi-quantitative explanation of these cracked tiny pit formations is put forward in §3-2.3. Other topographical features observed are:

[Pd/H_2O, D_2O/H_2SO_4/Pt//SEM, EDS//Surface pits with sub-micron size]. [4]

[Pd/D_2O/H_2SO_4/Pt//SEM, EDS//Blob and fibers]. [5]

[Pd/D_2O/H_2SO_4/Pt//SEM, EDS//New features]. [7]

[Ti/D_2O/H_2SO_4/Pt//EDS//Bubbles, craters and pits]. [9]

[Ti/D_2O/H_2SO_4/Pt//EDS//Valleys 4 μm deep with rims]. [10]

[Ni/H_2O/U_3O_8, HNO_3/Pt//SEM, EDS//Donut-like feature and voids with rims]. [11]

2.2 EXCESS HEAT [3, 4, 6-8, 10]

Excess heat (Q) has been found in both open and closed systems.

[Pd/H_2O, D_2O/H_2SO_4/Pt//SEM, STM, AFM//Closed//Q]. [1]

[Pd/H_2O/H_2SO_4/Pt//Closed//Q]. [3]

[Pd/H_2O, D_2O/H_2SO_4/Pt//Closed//Q]. [4]

This data demonstrates that the cold fusion phenomenon is not confined to deuterium systems, but can happen in Protium systems as well.

[Pd/D_2O/H_2SO_4/Pt//Closed//Q1 and Pt + Pd/SO_4/D_2O/H_2SO_4/Pt//Closed//Q_2, $Q_1 \approx Q_2$]. [6]

Clearly surface layers play a very important role in the CFP.

[Ti/D_2O/H_2SO_4/Pt//Closed//Q = 1.15 W]. [7]

[Pd/D_2O/H_2SO_4/Pt//Closed//Q = 5 W/g for 70 h]. [8]

[Ti/D_2O/H_2SO_4/Pt//Closed// In this particular experiment Q appears to depend on the degree of cold rolling of the cathodes]. [10]

2.3 Nuclear Transmutation (NT), NT_D [3 - 5, 7 - 10], **NT_F** [11]

Byproducts of nuclear transmutations have been spotted in the surface layers of the cathodes with the use of an energy dispersive spectrometer (EDS) and/or a secondary ion mass spectrometer (SIMS).

[Pd/H_2O, D_2O/H_2SO_4/Pt,//EDS//Au, Ag]. [3]

[Pd/H_2O, D_2O/H_2SO_4/Pt,//EDS//Cl, Ag]. [4]

This was, as far as we know, the first observation in a cold fusion phenomenon of new localized elements in the surface layer of the cathode.

[Pd/D_2O/H_2SO_4/Pt,//EDS//Ti, Al, Ag, Cd. An interesting after-effect was found in this experiment: Cd was produced 15 months after the end of the electrolysis.]. [5]

[Ti/D_2O/H_2SO_4/Pt,//EDS//V, Cr]. [7]

[Pd/D_2O/H_2SO_4/Pt,//EDS, SIMS//Cl. The relative abundance of Pd isotopes in the surface layer of cathodes was measured by SIMS.] [8]

The change of the relative abundance will be analysed in §3.2.2 using the TNCF model.

[Ti/D_2O/H_2SO_4/Pt,//EDS// Relative concentrations of $^{A}{}_{22}Ti$ changed] [9]
Ratios of titanium isotopes before and after experiments are shown in Table 1.

The TNCF model as shown in §3.2.1 qualitatively explains these changes.
[Ti/D_2O/H_2SO_4/Pt,//EDS//Cr, Fe]. [10]

Table 1: ICP/MS Results of Ti Cathode Before and After Experiments [9]

	Ti Cathode before	Ti Cathode after	Electrolyte after electrolysis
$^{50}Ti/^{46}Ti$	0.6960	0.6683	0.6593
$^{50}Ti/^{47}Ti$	0.8027	0.6978	0.7022
$^{50}Ti/^{48}Ti$	0.0785	0.0727	0.0685
$^{50}Ti/^{49}Ti$	1.0111	0.9358	0.9476

[Ni + U_3O_8/H_2O/H_2SO_4/Pt//EDS, ICP/MS//Cs, Fe, Ni. The most noteworthy and puzzling observation in this experiment was a change in the effective decay rate of uranium]. [11]

3. ANALYSIS OF THE EXPERIMENTAL DATA SETS BY THE TNCF MODEL

The TWF model as shown in this section consistently explains the experimental data sets introduced in the preceding section. The model assumes existence of quasi-stable thermal neutrons (trapped neutrons) with a density n_n in solids where the CFP occurred. These trapped neutrons likely originate from the tepid and more or less homogeneous bath of thermal neutrons that fills the Earth's atmosphere. They are regularly replenished by cascading collisions of high-energy cosmic rays with molecules of N_2 and O_2 in the upper layers. These trapped thermal neutrons induce nuclear reactions in the deuterons and/or protons composing the solid. The neutrons in the lattice become excited and form neutron bands (neutron valence bands) in which the density of neutrons can easily reach 10^{13} cm^{-3} if the excitation affects as little as one millionth of the nuclei in the solid. Subsequently, there ensues local coherence of the neutron Bloch waves at the boundaries of the sub-microscopic crystal regions. This local coherence effect brings as a consequence an intensification of the trapped thermal neutron density in the surface layer, something that impacts the surface topography then observed with the microscope.

In §3.1, a few qualitative features of the observed nuclear transmutations are explained with the reactions in Eqs. (2) – (21). Then, in §3.2, we will use Eq. (1) to account semi-quantitatively for the isotope ratio changes in Ti and Pd and topographic change of the cathode surface.

3.1 Qualitative Explanation of Experimental Data on Nuclear Transmutation

The overall features of nuclear transmutations, which were observed in the experiments summarized in Section 2.3, are consistently explained by using the reactions listed in Eqs. (2) - (20).

Production of new elements 1) V and Cr from Ti, 2) Ag and Cd from Pd, 3) Au from Pt, and 4) Cl from S is naturally explained by the nuclear transmutation by decay (NT_D) of lattice nuclei upon the absorption of neutrons.

Cl observed in experiments [3,8] is the result of Eq.(3). V and Ci observed in experiments [7] are the results of Eqs.(6) and (7), respectively.
Ag observed in experiments [3 – 5] is the result of Eqs. (13) and (15).

Cd observed in experiment [5] is the result of Eqs. (14) and (16).
Au observed in experiment [4] is the result of Eq. (19).
Furthermore, Al and Ti in experiment [5] may be the result of Eqs.(2), (4) and (5) due to minor elements Mg and Ca dissolved from the glass wall of the electrolysis cells.

On the other hand, in the data obtained in experiments with uranium,[11] there is the "decay-time shortening" observed already several times in CFP (Reference [12] §§11.7f, 11.11a, 11.11c). The intensification of radioactivity of uranium is explained by shortening of decay constants of uranium isotopes due to interactions of uranium nuclei with trapped neutrons.

There are also new elements explained by nuclear transmutation by fission (NT_F). The elements Cs, Fe, and Ni could be products of fission reactions of uranium isotopes after the absorption of neutrons as explained in the TNCF model. [12,14]

3.2 Quantitative Explanation of Experimental Data Sets

There are many features of CFP in the experimental data sets introduced in Section 2 to be analysed by a model to show the capability of the model and also a consistent explanation of whole data sets. In this Subsection, we take up two data sets of Ti and Pd isotope ratio changes and one of surface microstructure formation to give quantitative analysis.

3.2.1 Quantitative Explanation of Experimental Data on the Isotope Ratio Change of $^{A}_{22}$Ti

To analyse the quantitative data of the change of Ti isotope ratios, [9] we give the necessary equations deduced from the fundamental formula (Eq.(1)) as follows. After an experiment, of a time τ, the density x_i (i = 1 - 5) of isotopes $^{A}_{Z}$Ti (A= 46–50) changes by the absorption of a neutron, and also β-decay (or electron capture (EC)) according to following equations (cf. Eq.(1)):

$$x_1 = x_1^{(0)} - 0.35 n_n v_n \sigma_1 \tau x_1^{(0)} \tag{22}$$

$$x_i = x_i^{(0)} + 0.35 n_n v_n \sigma_{i-1} \tau x_{i-1}^{(0)} - 0.35 n_n v_n \sigma_i \tau x_i^{(0)}, \qquad (i = 2 - 5) \tag{23}$$

where we simplified the relation by taking V= 1 and ξ= 1 in Eq.(1). These quantities are irrelevant in calculating ratios of densities of isotopes- It is also assumed that the total number of titanium nuclei with mass numbers A = 46 – 50 do not change as a whole. In these equations, the fusion cross-sections of a thermal neutron and Ti isotopes $^{A}_{Z}$Ti (A = 46 – 50) are written as σ_i (i = 1 - 5), respectively. The values of σ_i are tabulated in Table 2.

Table 2: Thermal neutron capture cross-section of titanium isotopes $^{A}_{Z}$Ti in barns (b).
1 b = 10^{-24} cm^2.

A	46	47	48	49	50
i	1	2	3	4	5
$\sigma_{n-^{A}Ti} \equiv \sigma_i$	0.596	1.702	7.844	2.214	0.179

Then, we can write down the ratio $\eta_{5i} \equiv x_5/x_i$ (i = 1 - 4) using the initial ratio $\eta_{5i}{}^{(0)} \equiv x_5{}^{(0)}/x_i{}^{(0)}$ as follows, where the abbreviation $a = 0.35; 35 n_n v_n \tau$;

$$\eta_{51} \equiv x_5/x_i = (x_5{}^{(0)} + a(x_4{}^{(0)}\sigma_4 - x_5{}^{(0)}\sigma_5))/(x_1{}^{(0)} - x_1{}^{(0)}\sigma_1) = (\eta_{51}{}^{(0)} + a(\eta_{41}{}^{(0)}\sigma_4 - \eta_{51}{}^{(0)}\sigma_5))/(1-a\sigma_5) \quad (24)$$

$$\eta_{5i} \equiv x_5/x_i = (x_5{}^{(0)} + a(x_4{}^{(0)}\sigma_4 - x_5{}^{(0)}\sigma_5))/(x_i{}^{(0)} - a(x_{i-1}{}^{(0)}\sigma_{i-1} - x_i{}^{(0)}\sigma_i) = (\eta_{5i}{}^{(0)} + a(\eta_{4i}{}^{(0)}\sigma_4 - \eta_{5i}{}^{(0)}\sigma_5))/(1 - a(\eta_{i-1,i}{}^{(0)}\sigma_{i-1}\ \sigma_i) \quad (25)$$

From these equations, we can calculate $\eta_{5i}|_{th}$ (i = 2 - 4) using the experimental value of $\eta_{51}|_{ex}$ = 0.6683 (in Table 1) to compare $\eta_{5i}|_{ex}$ (i = 2 – 4).

The first equation determines the value a by using experimental values of η_{51}, $x_1{}^{(0)}$, $x_4{}^{(0)}$, and $x_5{}^{(0)}$ and the cross section σ_1, σ_4, and σ_5 given in Table 2;

$$a = (\eta_{51}{}^{(0)} + \eta_{51})/(\eta_{41}{}^{(0)}\sigma_4 + \eta_{51}{}^{(0)}\sigma_1 - \eta_{51}{}^{(0)}\sigma_5) = 0;.183\sigma_4{}^{-1} \quad (26)$$

Using this value of a in the equation (25), we can calculate $\eta_{5i}|_{th}$ (i = 2 - 4) and the result is tabulated in Table 3. Table 3 also has the tabulated initial concentrations $x_i{}^{(0)}$ of titanium isotopes ${}^{A}{}_{Z}\mathrm{Ti}$ (A = 46 – 50 ≡ i = 1 – 5), which is assumed to be the natural abundance that is tabulated in the first column. Nominal ratios $x_5{}^{(0)}/x_i{}^{(0)}|_{nom}$ are calculated and tabulated in the second column to be compared with the experimental ratio $x_5{}^{(0)}/x_i{}^{(0)}|_{exp}$ in the third column that was obtained in Table 1.

Table 3. Data about titanium isotopes ${}^{A}{}_{Z}\mathrm{Ti}$ (A = 46 – 50 ≡ i = 1 - 5) in cathodes. Natural abundance $x_i{}^{(0)}$, nominal abundance ratio $\eta_{5i}{}^{(0)}|_{nom} \equiv x_5{}^{(0)}/x_i{}^{(0)}|_{nom}$, measured ratio $\eta_{5i}{}^{(0)}|_{exp} \equiv x_5{}^{(0)}/x_i{}^{(0)}|_{exp}$ after experiments, and their theoretical value $\eta_{5i}|_{th}$ after experiments calculated using $\eta_{5i}{}^{(0)} \equiv x_5{}^{(0)}/x_i{}^{(0)}|_{exp}$.

Isotope	$x_i{}^{(0)}\|_{nom}$ (%)	$x_5{}^{(0)}/x_i{}^{(0)}\|_{nom}$	$x_5{}^{(0)}/x_i{}^{(0)}\|_{exp}$	$\eta_{5i}\|_{exp}$	$\eta_{5i}\|_{th}$
^{46}Ti (i = 1)	7.93	0.6734	0.6960	0.6683	(0.6683)
^{47}Ti (i = 2)	7.28	0.7335	0.8027	0.6978	0.771
^{48}Ti (i = 3)	73.94	0.0722	0.0785	0.0727	0.0846
^{49}Ti (i = 4)	5.51	0.969	1.0111	0.9358	0.402
^{50}Ti (i = 5)	5.34	1.000	(1.0000)	(1.000)	(1.000)

The rather large difference of $\eta_{54}|_{exp}$ and $\eta_{54}|_{th}$ is partly explained by the assumption in Eq.(22) that x_4 is determined by $x_3{}^{(0)}$ that should be replaced by x_3 to give correct value. By the large cross-section given in Table 2 and large natural concentration, x_3 is subject to large change in the course of experiments. This causes the rather small value of $\eta_{54}|_{th}$ which was calculated using Eq.(22).
The value a gives the parameter n_n of the TNCF model as follows;

$$a = 0.35 n_n v_n \tau,$$

or

$$n_n = a/0.35 v_n \tau \quad (27)$$

Using the values $v_n = 2.2 \times 10^5$ cm/s for thermal neutrons at room temperature, experimental -value of $\tau = 1$ day $= 8.64 \times 10^4$ s, $\sigma_4 = 2.2 \times 10^{-24}$ cm^2, and the above determined value $a = 0.183\ \sigma_4^{-1}$, we obtain

$$n_n = 1.25 \times 10^{13} \quad (\text{cm}^{-3}). \tag{28}$$

This value is in the highest range of values determined for about 60 experimental data sets. [12, 13]

3.2.2 Quantitative Explanation of Experimental Data on the Isotope Ratio Change of $^{A}{}_{46}$Pd

The experimental data on the relative abundance of Pd isotopes by SIMS given in the Figures 1(a) and (b) in the paper [8] can be summarized as given in Table 4.

Table 4: Data about palladium isotopes $^{A}{}_{Z}$Pd (A = 102 - 110 ≡ i = 1 - 6) in cathodes- To calculate experimental values of relative composition, we used SIMS data at 0.09 μm from the surface (15 minutes from the beginning). Natural abundance $x_i^{(0)}$, nominal abundance ratio $\eta_{i1}^{(0)}|_{nom} \equiv x_i^{(0)}/x_1^{(0)}|_{nom}$, measured ratio $\eta_{i1}^{(0)}|_{exp} \equiv x_i^{(0)}/x_1^{(0)}|_{exp}$ before and $\eta_{i1}|_{exp} \equiv x_i/x_1|_{exp}$ after experiments, and their theoretical value $\eta_{i1}|_{th}$ after experiments calculated using $\eta_{21}^{(0)} \equiv x_2^{(0)}/x_1^{(0)}|_{exp}$.

Isotope (i)	σ_i (b)	$x_i^{(0)}\|_{nom}$ (%)	$\eta_{i1}^{(0)}\|_{nom}$	$\eta_{i1}^{(0)}\|_{exp}$	$\eta_{i1}\|_{exp}$	$\eta_{i1}\|_{th}$
^{102}Pd (i = 1)	3.36	0.96	1.000	1.000	1.000	(1.000)
^{104}Pd (i = 2)	0.523	10.97	11.42	9.0	13.7	(13.7)
^{105}Pd (i = 3)	20.25	22.33	23.26	19.8	25.0	7.9
^{106}Pd (i = 4)	0.303	27.33	28.47	24.0	27.8	51
^{108}Pd (i = 5)	8.504	26.71	27.82	23.8	32.8	18
^{110}Pd (i = 6)	0.227	11.81	12.30	9.5	14.8	12

To analyze the quantitative data of the change of Pd isotope ratio, [8] we use similar equations as, Eqs.(22) and (23). For isotopes with large capture cross sections i = 4 and 5, it is necessary, however, to use exponential functions

$$x_i(t) = x_i^{(0)}\, e^{-a\sigma t}, \tag{29}$$

instead of the approximate linear function $x_i^{(0)}(1 - a\sigma t)$ used in Eqs. (22) and (23).

Results of calculation are given in the last column of Table 4, using the value of i = 2 for determination of the parameter a, to be compared with the experimental values in the 5th column. The comparison shows semi-quantitative coincidence except the values of i = 4 and 5, which we assumed the data were exchanged, and showed that the ratio of $^{106}{}_{46}$Pd/$^{108}{}_{46}$Pd changed to be less than 1 from the natural value of 1.023. As shown in this analysis, the ratio should be larger than natural value to be consistent with other data. The value of a determined by the data of i = 2 is expressed as follows:

$$a = 5.8 \times 10^{22}\ \text{cm}^{-2} \tag{30}$$

This value of a determines the parameter n_n if we know values of the quantities appearing in Eq. (27). If we take the experimental time of 12 minutes written in the paper [8] as the value of τ, we obtain

$$n_n = 1.0 \times 10^{15} \text{cm}^{-3} \tag{31}$$

While if we use another value $\tau = 7.5$ years $= 2.37 \times 10^8$ s, suggested by the elapsed time between the electrolysis experiment on April 24, 1989 and the SIMS measurement on October 4, 1996, we obtain a value

$$n_n = 3.18 \times 10^9 \text{cm}^{-3}. \tag{32}$$

There are many observations of after effects in cold fusion experiments including the one described in reference [5]. Some reactions proceed once necessary conditions for CFP are established in the material.

On the other hand, the excess heat was also measured in this experiment: [8] the excess heat measured in a Pd foil cathode of 0.055 g and surface area 2 cm^2 was 5 W. If we assume the excess heat was generated by reactions (34) and (35), explained next in subsection 3.2.3, occurring in the surface layer of a thickness 1 μm with a composition $PdH_{0.5}D_{0.5}$, we obtain a value of n_n of

$$n_n = 4 \times 10^{12} \text{ cm}^{-3} \tag{33}$$

This value compares with those values given in Eqs. (31) and (32) and shows that the reactions causing the change of isotope ratios occurred in a longer time period than duration of the experiment (12 minutes), but shorter than the interval of two measurements (7.5 years) and in about 2.4×10^5 seconds (3 days), if n_n did not decay in this period.

3.2.3 Quantitative Explanation of Pit Formation in the Surface Layer of Cathodes

To analyze the microstructure of the cathode surface after electrolytic experiments, we take up the data given in reference [2].

According to the TNCF model, we assume the existence of trapped neutron in the material with a density n_n, which is taken as an adjustable parameter. The trapped neutrons are quasi-stable to react with particles in the surface layer where the parameter $\xi = 1$ in Eq.(1).

As main reactions to explain the thermal effect which produces microscopic craters in the surface region, we take reactions with protons and deuterons occurring in a localized region by some causes (suggested by experimental results [1 – 5]):

$$n + p = d + Q_1, \tag{34}$$

$$n + d = t + Q_2 \tag{35}$$

where $Q_1 = 2.2$ MeV and $Q_2 = 6.25$ MeV are absorbed by particles in solids while they are emitted as photons in reactions occurring in free space. We can ignore reactions with palladium isotopes due to the negligible amount of energy liberated in them compared with the above two reactions.

This assumption is suggested by our theoretical prediction of high-density neutrons [17] and neutron drops [18] formed in near-surface layers which interact especially with hydrogen isotopes therein, and induce reactions (34) and (35), giving the liberated energy Q_1 and Q_2 to the many body system made of lattice nuclei (Pd), occluded hydrogen isotopes (D and H), and neutron drops.

Assume a crater is made by the localized heating of a sphere S with a radius r_m at a point P, some distance d ($> r_m$) below the surface layer of the cathode (Fig.1). Let us assume heating occurs by localized heat generation in the sphere, with a constant rate q (J/s) and dissipation q' (.J/s) of thermal energy through the surface S with an area $4\pi r_m^2$ by heat conduction.

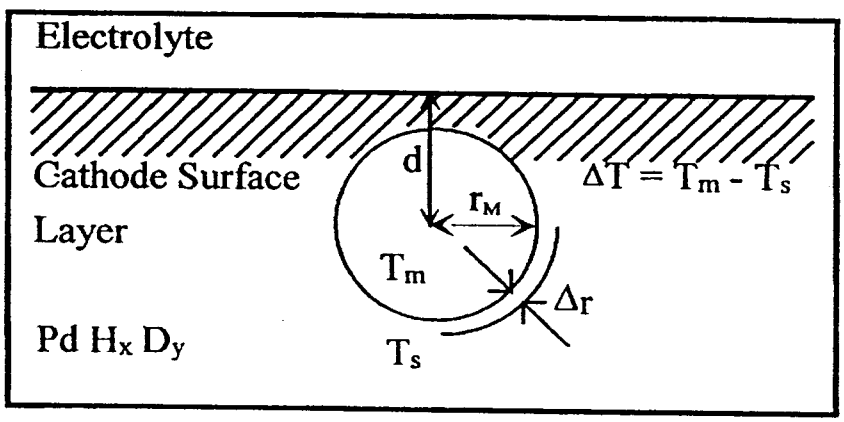

Fig. 1 A model for localized melting of sphere S in the surface layer of a Pd cathode occluding hydrogen and deuterium as PdH_xD_y. When the sphere S melts at or near the surface and is superheated above the boiling point of the constituent material by nuclear reactions occurring therein, an explosion occurs, thus forming a crater or a pit with various shapes depending on the parameters of the droplet and matrix.

We assume the composition of the cathode material in the surface layer to be PdH_xD_y. Reactions (34) and (35) which occur in a unit time are given by Eq. (1) with appropriate parameters for both the proton and the deuteron. Their reaction cross-sections are 0.332 and 5.5 x 10^{-4} b, respectively (1 b = 10^{-24} cm^2). Then, we can write the heat generation rate q as follows:

$$q \equiv -q_1 + q_2 = N_{np}Q_1 + N_{nd}Q_2, \tag{36}$$

where Nnp and Nnd are given by Eq.(1) using $\xi = 1$ (by a premise in the TNCF model), $V = (4\pi/3)r_m^3$, $n_p = x\, n_{Pd}$ and $n_d = y\, n_{Pd}$, and $n_{Pd} = 6.88 \times 10^{22}$ cm^{-3}, and thermal velocity of neutrons $v_n = 2.2 \times 10^5$ cm/s.

To calculate the dissipation rate q', we replace physical parameters, thermal conductivity κ and heat capacity c_m of PdH_xD_y by those for palladium metal, for simplicity, allowing ambiguity factors of about two:

$$\kappa = 0.755 \text{ W/cm s K}$$

and

$$c_m = 25.9 \text{ J/K mol. (Pd)}$$

Then, the dissipation rate of heat through the surface of the droplet with an area $S = 4\pi r_m^2$ is given as

$$q' = \kappa S \Delta T / \Delta r \tag{37}$$

where Δr is the transition length of the temperatures from the inside one T_m to outside one T_s (~the room temperature). As the temperature difference ΔT between the melted sphere and the ambient solid of the cathode, we take $\Delta T = T_m - T_s = 2473$ (K)- 293 (K) = 2180 K taking T_m as the boiling point of palladium metal (we assume explosion of the super-heated droplet to form pits or craters at the cathode surface) and T_s as the room temperature.

As the distance Δr between the melted region of the droplet and the ambient solid, we may take a thin shell with a thickness of $10^{-2} r_m$, while the radius of the melted droplet r_m, can be taken as 1 μm as suggested by experimental results.[2]

Putting these values into Eq. (37), we obtain the heat dissipation rate as follows:

$$q' = 1.824 \times 10^{13} \text{ (MeV/s)}. \tag{38}$$

On the other hand, the heat generation rate (36) is rewritten as follows:

$$q = 2.22 \times 10^{-8} n_n (0.737x, + 0.00003436y) \text{ (MeV cm}^3\text{/s)}, \tag{39}$$

This relation shows rather effective role of protons than deuterons to produce excess heat if x and y have the same orders of magnitude.

To have an explosion of a droplet, it is necessary to have a rapid enough heat production over the dissipation and we can assume a condition for the explosion

$$q >> 10^2 q'. \tag{40}$$

Assuming further x = y = 0.5 for the composition of the surface layer, we can determine the extreme value of the heat generation q_{ext} defined by $q_{ext} = 10^2 q'$ using the value in Eq.(38)

$$\begin{aligned} q_{ext} &= 10^2 \, q' \\ &= 0\,81 \times 10^{-8} \, n_n \text{lext} \text{ (MeV cm}^3\text{/s)} \\ &= 1.824 \times 10^{15} \text{ (MeV/s)} \end{aligned} \tag{41}$$

On the other hand, we can estimate the time necessary to evaporate the droplet when the heat production rate is q_{ext}. The heat capacity of palladium is 25.9 J/K mol, heat of melting 167 kJ/mol = 1.67×10^4 J/mol and the droplet with a radius $r_m = 10^{-4}$ cm contain palladium atoms of 0.48×10^{-12} Mol. Therefore, the heat capacity of the droplet is 7.734 x 10 MeV/K and heat of melting is 4.999×10^4 MeV. These values give a time τl_{boil} necessary to boil the droplet by the heat generation rate q_{ext},

$$\tau l_{boil} = 1.58 \times 10^{-10} \text{ (s)}. \tag{42}$$

This is a short enough time the droplet explodes before the generated heat dissipates to the environment.

Furthermore, the relation (41) together with (38) give the value $n_n|_{ext}$ in Eq. (1) corresponding to the extreme heat generation Eq.(41)

$$n_n|_{ext} = 2.2 \times 10^{19} (cm^{-3}). \quad (43)$$

It is conceivable that such a large value of the parameter n_n occurs in extreme cases in localized regions. The averaged out events like excess heat, total amounts of ^{4}He and tritium have given values of n_n in the range of $10^8 - 10^{13}$ cm^{-3}. [12] The value of 10^{19} cm^{-3} obtained in the events of pit formation with extreme conditions at the surface can be interpreted only by the idea of the neutron valence band [19 – 21] developed recently using excited neutron states of lattice nuclei. Conversely, the occurrence of localized vaporization lends credibility to the theoretical treatment.

However, the use of rather common values obtained in analysis of many data sets and also in §3.2.1 and §3.2.2 give $n_n \sim 10^{13}$ cm^{-3}. Then the time τ necessary to evaporate the tiny droplet to make pits and craters is about 1 second. This is not inconsistent with assumptions made in the above treatment, e.g., Eq. (40), with some modifications of parameters r_m, S, Δr, and others. Thus, we can safely say that the TNCF model, consistently with other events of CFP, explains pits or craters found on the surface of cathodes.

4. CONCLUSION

The possible nuclear transmutations by decay (NT_D) and by fission (NT_F) in the surface layers of Pd, Ti and Ni cathodes which were observed by J. Dash et al. were consistently explained by the TNCF model except for the one case of the $^{106}_{46}$Pd/$^{108}_{46}$Pd ratio change.

The TNCF model successfully explained the overall changes of isotope ratios of titanium and palladium. This result suggests the reality of the existence of the "trapped neutrons" in the nuclear transmutations occurring in electrolytic experiments of CFP as already shown in our previous work. [12 – 14] The data concerning $^{106}_{46}$Pd/$^{108}_{46}$Pd ratio [8] is a riddle that is inconsistent with the TNCF model, even if the interchange of the data of $^{106}_{46}$Pd and $^{108}_{46}$Pd ratio [8] gives an apparently consistent result.

This inconsistency of the amount of $^{106}_{46}$Pd in experimental and theoretical data might be caused by theoretical assumption of only the reactions

$$n + {}^{105}_{46}\mathrm{Pd} = {}^{106}_{46}\mathrm{Pd} + \gamma \quad (44)$$

$$= {}^{105}_{46}\mathrm{Pd} + n' \quad (45)$$

Although a larger absorption cross section of 2.025 x 10 b for the reaction (44) over that of the inelastic reaction (45) is confirmed by experiment, we can imagine a possibility of having other reactions with larger branching ratios in solids than those in free space reducing population of $^{106}_{46}$Pd calculated on the assumption of Eq. (44) only to accord with experimental data. One example of this kind of reactions in free space is seen in the following thermal neutron-$^6_3$Li reactions:

$$n + {}^{6}_{3}\mathrm{Li} = {}^{7}_{3}\mathrm{Li} + \gamma \quad (46)$$

$$= {}^{3}_{1}\mathrm{H} + {}^{4}_{2}\mathrm{He} \quad (47)$$

where the branching ratios of these reactions are » 10^{-4} vs. 1 with the cross sections for the first and the second reactions are 3.85×10^{-2} and 9.4×10^{2} b, respectively.

It should be noticed here a possibility of multi-neutron or a neutron-proton cluster absorption from a neutron drop by a lattice nucleus. We have used only single neutron absorption reactions Eqs. (2) - (21) in the explanation of NT observed by Dash et al. [1 - 11]. The data showing Cd on Pd [5] and Cr on Ti [7, 10] however, are also explained by absorption of two neutrons followed by double beta-decays or by absorption of a cluster of two neutrons and two protons. Large changes of mass numbers have recently been reported: Iwamura et al. [21] reported NT's of Cs → Pr and Sr → Mo, Yamada et al. [22] reported NT's of Pd → Ba and Pb. These NT's could only be explained by absorptions of clusters (N_n, N_p) composed of N_n neutrons and N_p protons by a nucleus on the cathodes from a neutron drop. Suggested clusters are: (2,2), (4,4), (20±, 10), and (100±, 36). These possibilities will be discussed elsewhere. [23]

The unexplained riddle of the ${}^{106}_{46}\mathrm{Pd}/{}^{108}_{46}\mathrm{Pd}$ ratio [8] might be related with this cluster absorption by a lattice nucleus.

Specific features of topography changes are localized structures made by rapid super-heating in surface layers before dissipation of heat to surrounding parts. The quantitative treatment of crater formation given in Section 3.2.3 substantiates the reality of our model based on the participation of trapped neutrons in the CFP. The different shapes of craters observed in experimental data sets [1–5, 7–11] should be related with relative values of r_m, d, q, Δr, and ΔT. Blobs and fibres, [5] for instance, can be created by a slower heating rate of the droplet that does not explode but expands to make a hole through which melt flows out to the surface of the cathode and form a fibre. Details of topographical features will be a theme of a future work.

The appearance of the topographical features cited above suggests the possibility that reactions occurred in tiny regions in a short period of time. The localized high-densities of neutrons in boundary regions that were deduced in our papers [17,18] explain successfully and consistently the occurrence of nuclear reactions of this type. The local coherence of neutron Bloch waves at a boundary layer [17] results in a high density of neutrons therein. Then, the occurrence of trigger reactions at specific positions in the boundary layer, where there are high densities of neutrons, progress into breeding reactions to generate high energy nuclei and also produce high energy neutrons, which dissipate heat to the system as a whole.

The "after-effect" [5] observed in the Pd cathode shows clearly that the cold fusion phenomenon is not necessarily caused by electrolysis itself but that it is induced in states formed in the process of electrolysis. The same effect seems to work in the data set [8] to give NT_D to be consistent with the excess beat. Furthermore, this effect has appeared in a series of events known by the names "heat after death" and aging effect (cf. Reference [12] §6.4a and §7.2a) that were explained by the TNCF model. The after-effect observed by Miguet and Dash [5] is explained as follows: The surface of the Pd cathode formed in the process of electrolysis contains the necessary conditions for CFP, resulting

in the production of Ag by the reactions (13) and (15). The structure remained long after the experiment, resulting in induced nuclear transmutations to produce Cd by reactions (14) and (16).

ACKNOWLEDGMENT

This work is supported by a grant from the New York Community Trust snf by the Professioonal Development Fund for part-time faculty of Portland State University.

REFERENCES

1. J. Dash, P.S. Keefe, E. Nicholas, D.S. Silver, "Comparison of Light and Heavy Water Electrolysis with Palladium Cathodes," *Proc. of AESF 80th Annual Conference* (Orlando, Florida, June 1993), p 755 (1993).
2. D.S. Silver, J. Dash, P.S. Keefe, "Surface Topography of a Palladium Cathode after Electrolysis in Heavy Water," *Fusion Technology,* vol 24, p 423 (1993).
3. J. Dash, G. Noble, D. Diman, "Surface Morphology and Micro-composition of Palladium Cathodes after Electrolysis in Acidific Light and Heavy Water," *Proc. of 4th International Conference on Cold Fusion*, vol 2, p 25-1 (1993).
4. J. Dash, G. Noble, D. Diman, "Changes in Surface Topography and Micro-composition of a Palladium Cathode caused by Electrolysis in Acidific Light Water," *Cold Fusion Source Book* (Proc. Intn'l Symp. Cold Fusion & Advance Energy Sources, Minsk, Belarus), p 172 (1994).
5. S. Miguet, J. Dash, "Microanalysis of Palladium after Electrolysis in Heavy Water," *Proc. of 1st Low Energy Nuclear Reactions Conference,* College Station, Texas, p 23 (1995).
6. G. Noble, J. Dash, M. Breiling, L. McNasser, "Electrolysis of Heavy Water with a Palladium and Sulphate Composite," *Proc. of 5th International Conference on Cold Fusion* p 136 (1995).
7. R. Kopecek and J. Dash, "Excess Heat and Unexpected Elements from Electrolysis of Heavy Water with Titanium Cathodes," *Proc. of 2nd Low Energy Nuclear Reactions Conference,* College Station, Texas, p 46 (1996).
8. J. Dash, "Chemical Changes and Excess Heat caused by Electrolysis with H_2SO_4-D_2O Electrolyte," *Proc. of 6th International Conference on Cold Fusion, vol* 2, p 477 (1996).
9. M.K. Klopfenstein, J. Dash, "Thermal Imaging during Electrolysis of Water with a Ti Cathode," *Proc. of 7th International Conference on Cold Fusion*, p 98 (1998).
10. J. Warner, J. Dash, "Heat Production during the Electrolysis of D_2O with Titanium Cathodes," *Proc. 8th International Conference on Cold Fusion,* Lerici, Italy), p 161 (2000).
11. G. Goddard, J. Dash and S. Frantz, "Characterization of Uranium Co-deposited with Hydrogen on Nickel Cathodes," *Transactions of the American Nuclear Society*, vol 83, p 376 (2000).
12. H. Kozima, Discovery of the Cold Fusion Phenomenon – Evolution of the Solid State-Nuclear Physics and the Energy Crisis in 21st Century, Ohtake Shuppan KK. Tokyo, Japan, 1998.
13. H. Kozima, "TNCF Model – A Phenomenological Approach," *Proc. of 8th International Conference on Cold Fusion),* p 461 (2000).
14. H. Kozima, M. Ohta, K. Arai, M. Fujii, H. Kudoh, K. Yoshimoto, "Nuclear Transmutation in Solids Explained by TNCF Model," *Proc. of 8th International Conference on Cold Fusion),* p 455 (2000).
15. R.B. Firestone, Table of Isotopes, 8th edition, Wiley-Interscience, 1996.

16. H. Kozima, J. Warner, C. Salas Cano, J. Dash, "Consistent Explanation of Topography Change and Nuclear Transmutation in Surface Layers of Cathodes in Electrolytic Cold Fusion Experiments," *Proc. ICCF9* (2002) (to be published).
17. H. Kozima, K. Arai, M. Fujii, H. Kudoh, K. Yoshimoto, K. Khaki, "Nuclear Reactions in Surface Layers of Deuterium-Loaded Solids," Fusion Technol., vol 36, p 337 (1999).
18. H. Kozima, "Neutron Drop; Condensation of Neutrons in Metal Hydrides and Deuterides," *Fusion Technol.*, vol 37, p 253 (2000).
19. H. Kozima, J. Warner and C. Goddard, "Cold Fusion Phenomenon and Atomic Processes in Transition- Metal Hydrides and Deuterides," *J. New Energy*, vol 6-2, p 126 (2002).
20. H. Kozima, "Anomalous Nuclear Reactions and Atomic Processes in Transition-Metal Hydrides and Deuterides," *J. New Energy*, vol 6, no 3, pp 97-102 (2002).
21. H. Kozima, "Excited States of Nucleons in a Nucleus and Cold Fusion Phenomenon in Transition- Metal Hydrides and Deuterides," *Proc. ICCF9* (2002) (to be published).
22. Y. Iwamura, M. Sakano, T. Itoh, "Elemental Analysis of Pd Complexes Effects of D_2 Gas Permeation," *Jpn. J. Appl. Phys.*, vol 41, p 4642 (2002) (Cs → Pr, Sr → Mo).
23. H. Yamada, S. Narita, Y. Fujii. T. Sato, S. Sasaki, T. Omori, "Production of Ba and Several Anomalous Elements in Pd under Light Water Electrolysis," *Proc. ICCF9* (to be published); *Abstracts of ICCF9*, p 123 (2002). (Pd → Ba, Pb).
24. H. Kozima, "Production of Larger Mass-Number Nuclides in CFP," *Proc. 4-th Meeting* of *Japan CF Society* (JCF4) (to be published).